Journal Pre-proof



Assessment of mechanical properties of SPS-produced tungsten including effect of neutron irradiation

D. Terentyev, Monika Vilémová, Chao Yin, Jakub Veverka, Andrii Dubinko, Jiří Matějíček

PII: S0263-4368(19)30550-5

DOI: https://doi.org/10.1016/j.ijrmhm.2020.105207

Reference: RMHM 105207

To appear in: *International Journal of Refractory Metals and Hard Materials*

Received date: 8 July 2019

Revised date: 14 January 2020

Accepted date: 18 January 2020

Please cite this article as: D. Terentyev, M. Vilémová, C. Yin, et al., Assessment of mechanical properties of SPS-produced tungsten including effect of neutron irradiation, *International Journal of Refractory Metals and Hard Materials*(2020), https://doi.org/10.1016/j.ijrmhm.2020.105207

This is a PDF file of an article that has undergone enhancements after acceptance, such as the addition of a cover page and metadata, and formatting for readability, but it is not yet the definitive version of record. This version will undergo additional copyediting, typesetting and review before it is published in its final form, but we are providing this version to give early visibility of the article. Please note that, during the production process, errors may be discovered which could affect the content, and all legal disclaimers that apply to the journal pertain.

© 2020 Published by Elsevier.

Journal Pre-proof

Assessment of mechanical properties of SPS-produced tungsten including effect of neutron irradiation

D. Terentyev[1], Monika Vilémová[2], Chao Yin[1,3], Jakub Veverka[2,4], Andrii Dubinko[1], Jiří Matějíček[2]

[1] Structural Materials Group, Institute of Nuclear Materials Science, SCK•CEN, 2400 Mol, Belgium
[2] Institute of Plasma Physics, The Czech Academy of Sciences, 18200 Prague, Czech Republic
[3] Institute of Mechanics, Materials and Civil Engineering, Université Catholique de Louvain, 1348 Louvain-la-Neuve, Belgium
[4] Faculty of Nuclear Sciences and Physical Engineering, Czech Technical University in Prague, 11519 Prague, Czech Republic

CRediT author statement

Individual author contributions:

D. Terentyev: Conceptualization, Writing - Original Draft, Writing - Review & Editing

Monika Vilémová: Conceptualization, Investigation

Chao Yin: Investigation

Jakub Veverka: Investigation

Andrii Dubinko : Investigation

Jiří Matějíček: Writing - Review & Editing

Journal Pre-proof

Journal Pre-proof

Abstract

Production and supply of tungsten for the first wall fusion application is becoming an important aspect given the progress of ITER construction. Exploration of advanced routes alternative to the conventional powder metallurgy is currently undertaken. In this work we have assessed a potential of the spark plasma sintering (SPS) production route to deliver well controlled microstructure, chemistry and mechanical properties of bulk tungsten as a first step. SPS-produced tungsten was sintered at 2000°C and was characterized in terms of mechanical properties, namely: tensile, three point bending and fracture toughness data in the temperaure range of 250-600°C. Then, neutron irradiation was performed at 600°C and the change of the fracture toughness was measured after irradiation together with the characterization of the fracture surface. The results are compared with those obtained for the commerically produced swaged tungsten irradiated and tested in equivalent conditions. The obtained results show that SPS technology offers the production of bulk tungsten with a good potential for further optimization (by e.g. swaging/rolling). Neutron irradiation causes the reduction of the fracture toughness comparable to the one induced in the commercially produced tungsten.

Keywords: Tungsten, mechanical properties, neutron irradiation, fusion.

*responsible author, email: dterenty@sckcen.be

Journal Pre-proof

Journal Pre-proof

1. Introduction

Development of materials and composites for components to operate in nuclear fusion environment remains one of the hottest topics on the agenda of fusion electricity roadmap. In particular, harsh operation environment involving large thermal gradients, high number of thermal cycles and flux of fast neutrons inevitably leads to degradation of thermal, physical and mechanical properties of materials facing the plasma [1]. Following a thorough assessment, tungsten has been selected as first wall material for the divertor of ITER [2] and DEMO [3]. In the case of ITER lifespan, the total power load of divertor PFC is targeted as ~0.3 MW a m-2, which is equivalent to the irradiation dose of 1.35 dpa (displacement per atom) [4]. The PFC of ITER is planned for replacement three times during the life span, thus the equivalent end-of-operation irradiation dose is ~0.3-0.5 dpa during the D-T phase [5].

Compared to ITER, the operational conditions of DEMO are more demanding. The first wall armor and diverter will experience longer pulses (> 2 hours), higher heat flux load (MW/m^2) and correspondingly a higher total neutron fluence (up to 5 dpa in the strike point) [3]. While various routes may be applied to improve/optimize the material (e.g. alloying, secondary phase inclusion, fiber/laminar strengthening, additive manufacturing, etc.), in general the design of component must account for a number of constrains such as: efficient power exhaust (commercially viable), operational temperature window (compatible with coolant option), acceptable nuclear waste (economy, license), compatibility with plasma (low erosion, no plasma pollution), compatibility with fuel cycle (retention, breathing) and finally operation lifetime [6]. The latter is inherently linked to both safety and commercial viability aspects of the fusion nuclear power reactors. One of particular aspects that needs to be addressed for tungsten (W) as plasma-facing material is its mechanical properties, which are affected by neutron irradiation [5].

Overall, it is agreed that efficient application of W in fusion reactors will be determined by a best compromise between reduced DBTT and enhanced fracture toughness as well as high recrystallization temperature [7]. This is why advanced W-based grades as well as new manufacturing routes are under development to improve low- and high-temperature performance. For example, particle-reinforced tungsten and reduced grain size material can suppress the grain growth, improve the strength of grain boundary as well as fracture toughness of the material, and reduce DBTT (see reviews [6, 8]). Fiber-reinforced tungsten allows one to overcome the intrinsic brittleness of tungsten and its susceptibility to embrittlement induced under operation, as W fibers arrest and deflect the propagating cracks (see e.g. [9, 10]). By dedicated alloying with zirconium-carbon (ZrC) nano-sized particles as well as by applying the powder metallurgical process, it was possible to reduce the free oxygen occupying grain boundaries and successfully fabricate bulk plate of W-0.5wt.%ZrC alloy [11].

Production of tungsten grades relevant for ITER applications consists of several steps, including preparation of green compact at room temperature, conventional sintering at temperatures above 2200 °C, subsequent thermo-mechanical treatment (rolling or forging) and final thermal treatment for stress relief. Such a multi-step process is time demanding and increases the price of the final product. Therefore, tungsten-based material development and investigation of alternative production routes is undergoing with the aim to simplify the production route and improve the mechanical response of the material. Several promising manufacturing routes are currently investigated, each offering specific advantages. Among these methods are powder/metal injection molding delivering net-shaped compacts with the help of polymer binders [12], thermal spray methods producing coatings over large

areas (see e.g. [13, 14]). Most recently, cold spray was used to produce dense tungsten coatings with minor Ti binder, offering the advantage of spraying in ambient air without apparent tungsten oxidation and excellent adhesion to the substrate material (J.Cizek and M. Vilemova, to be published soon). The powder consolidation method used in this study belongs to the family of sintering methods. The advantages of the SPS process are fast heating rates and very short hold times at the sintering temperatures (in the range of several minutes). Therefore, fine grain structure of the original powder can be preserved. During the sintering, uniaxial pressure can be applied and various sintering atmospheres can be used to influence the resulting microstructure and purity of the compacts.

Fracture toughness (FT) is one of the most important and relevant material characteristic, describing material response and behaviour in the presence of crack. According to the material resistance to crack propagation, brittle and ductile materials are distinguished. For many materials, including tungsten, particular temperature can be determined, above which the material responds in ductile way. This temperature is often denoted as ductile to brittle transition temperature (DBTT). For tungsten, the DBTT and generally the behaviour strongly depends on the fabrication route, related microstructure, impurities and thermal history (e.g. recrystallization temperature is of greatest importance).

In the case of commercially pure tungsten, it has been shown that at room temperature the FT value is about 5-10 MPa$\sqrt{m}$ and it rises up to 20-25 MPa$\sqrt{m}$ [15-17] as temperature exceeds 300-350°C which can be seen as transition from ductile to brittle fracture mode in polycrystalline tungsten, following the results of tensile tests and subsequent fracture surface analysis [18].

Without any post-treatment, the DBTT of commercially pure tungsten usually falls in the region of 300-600°C or higher [19-22]. Given thermo-mechanical treatment (e.g. hot/cold rolling, swaging, forging etc.), the DBTT can be decreased down to as low as room temperature (RT) for tungsten in the form of foil/thin sheet or down to 80-350°C for bulk products [23-29]. Following the above cited works, fracture toughness of bulk polycrystalline tungsten without post production treatment is about 5-10 MPa$\sqrt{m}$ in the brittle region and it increases to ~20 MPa$\sqrt{m}$ in the transition region. After rolling, the values were similar, only shifted to the lower temperatures [28]. In case of ultra-fine grain (UFG) tungsten foil [30], in brittle region fracture toughness K_Q reached values of about 10 MPa $\sqrt{m}$ with increase to around 50 MPa$\sqrt{m}$ in the ductile region. Of particular example of the reduction of DBTT is the work of Bonnekoh, Hoffmann and Reiser [24], in which the DBTT was measured to be as low as -65±15 °C, which was achieved through multiple rolling steps introducing significant deformation and reducing the thickness as well as grain size.

Needless to say that mechanical properties of tungsten (and other metals), including fracture toughness and DBTT, can be affected significantly by neutron irradiation. The resulting microstructure consisting of point defects, dislocation loops, voids and precipitates is responsible for the degradation of the mechanical properties. Recently, hardness and tensile tests of single-grain tungsten samples after irradiation to 0.4 dpa at 690-800°C were performed in [31]. Whereas unirradiated samples exhibited ductility starting at 300°C, this shifted to above 500°C after the irradiation [32]. Steichen et al. measured DBTT shift of about 165°C (from 65°C to 230°C) of cold-pressed and sintered tungsten specimens irradiated to fluence of 0.9 x 10^{22} n/cm^2 [33]. Three point bending tests of tungsten (irradiated on the spallation neutron source) were performed by Habainy et al. [34]. The samples were irradiated by high-energy protons and spallation neutrons at temperatures up to 500°C and damage up to 3.5 dpa. Whereas DBTT of unirradiated specimens was around 350°C, all irradiated specimens exhibited brittle fracture at test temperatures up to 500°C. Finally, Gorynin et al. have studied mechanical properties of tungsten under neutron irradiation up to 2.2 x 10^{22} n/cm^2 by performing irradiation at 350, 500 and 800°C on BOR60 reactor and measuring tensile properties.

Fully brittle deformation was observed after irradiation at 500°C and below. As of today, the information on the change of the fracture toughness after neutron irradiation is not available in open literature up to the best knowledge of authors.

In this work, we perform a preliminary assessment of the mechanical properties of tungsten produced by SPS technology. Given a number of advantages of SPS including industrial scalability, cost effectiveness, flexibility for shape/alloying, we assess the mechanical properties of pure W produced by SPS in the temperature range up to 600°C including neutron irradiation. The choice of 600°C is driven by constrains originating from (i) the irradiation-induced void swelling above 650°C [35, 36] and compatibility with structural steels in location of joints [1]. The purpose of this work is to explore nominal performance of SPS-produced tungsten (i.e. without thermo-mechanical optimization) and compare the results with those available for commercially pure tungsten. The results include tensile, bending and fracture toughness tests in the as-received condition and fracture toughness tests for the material irradiated at 600°C up to 0.24 dpa, which is close to the half end-of-life fluence of tungsten PFC on ITER device (i.e. replacement of the PFC is scheduled at 0.4 dpa). The results are compared with data recently obtained for commercially pure W (produced by A.L.M) irradiated and tested in the equivalent conditions [37].

Journal Pre-proof

2. Experimental methodology and materials microstructure in as-produced state

2.1 SPS methodology and down-selection procedure to choose optimized sintering route

The samples were prepared from tungsten powders with a characteristic size of 2 µm (Global Tungsten & Powders, Bruntál, Czechia), using an SPS 10-4 (Thermal Technology, USA) spark plasma sintering equipment. The previous experience had shown that bending strength of the samples measured at room temperature increased with sintering temperature. Therefore, the samples were sintered at 2000 °C and 70 MPa. The grain growth caused by the high temperature was balanced by short sintering time, i.e. 2 minutes. Ar+7%H2 was used as sintering atmosphere in order to eliminate oxygen impurities at the grain boundaries by reducing effect of hydrogen gas. The evolution of temperature and pressure during the processing is shown in Fig.1. SPS compacts of 3.7 mm thickness and 15 mm diameter and 5.1 mm thickness and 30 mm diameter were used for the preparation of the fracture toughness and tensile specimens, respectively.

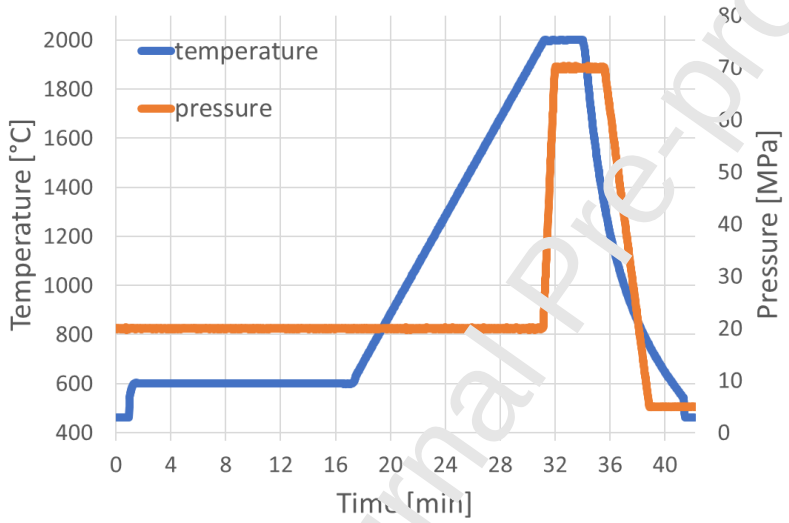


Fig.1. Evolution of temperature and pressure during the processing of the SPS tungsten material.

In addition to the above described SPS W, we will use the results obtained by us earlier for the commercially pure W grade. The material was fabricated in China by AT&M company by powder metallurgy production route (> 99.94 at.% purity) and normalized by rolling to achieve the microstructure according to the ITER specification [2]. The characterization of mechanical properties of this material was assessed in refs. [18, 22].

2.2 Microstructural characterization of the material

To provide a primary information on the microstructure of the fabricated material, scanning and transmission electron (SEM and TEM, respectively) was applied to screen the grain shape, size as well as microstructural features inside the grains. Surface imaging was performed using SEM JEOL 6610 with secondary electron detector (accelerating voltage 15 kV and working distance of 10-11 mm). Electron back scattering diffraction (EBSD) analysis was also performed. The grain orientation maps were obtained using Bruker Quantax software. The morphology of the SPS and commercial W grades are shown in Fig.2(a) and Fig.3(a), respectively. The morphology and grain size is analyzed and

calculated by MTEX plugin. As we can see, SPS W has uniform distribution of equiaxed grains with an effective grain size of ~9 µm. Commercial W has a strong texture with elongated grains (of pancake-like shape) parallel to the rolling direction. The equivalent size of the grain is ~60 µm.

Transmission Electron Microscopy (TEM) samples (10×3×1.25 mm) were extracted from the middle of the fabricated samples. The slices were mechanically polished from both sides using SiC paper to achieve 70-100 µm thickness and further cut with a wire cutter into pieces to fit 3 mm TEM grids. They were polished again from both sides with #4000 SiC paper to remove the remnants of glue, rinsed in acetone and ethanol and glued on 3 mm copper grids with an aperture of 1 mm. Finally, the specimens were polished electrochemically with a solution of 1.5 wt.% NaOH in water with an applied voltage of 30 V. The specimens were investigated in JEOL 3010 TEM operating at 300 kV. TEM was applied to screen the presence of sub-grains and to evaluate the dislocation density, which is why we provide only brief details and results to support general understanding of the microstructure of the SPS materials and the difference with the commercial W grade.

Bright field TEM images for SPS and commercial W are provided in Fig.2 (b,c) and Fig.3(b,c). SPS W microstructure consists mostly of well-defined high angle grain boundaries and triple junctions. Most of the dislocation lines observed had a straight-line shape. No sub grains were observed in the SPS tungsten. The microstructure of AT&M W consists of many sub-grains with a size of 0.5-3 µm. Sub-grains are separated by low-angle grain boundaries. Dislocations are often observed to be curved and in some regions dislocation tangles are also identified. These observations are consistent with the fabrication processes involving hot rolled deformation. The method, described in [38], was used to calculate the dislocation density. A circle was drawn randomly on a TEM image and the number of intersections of it with dislocation lines was counted. Dislocation density was then calculated as $\rho = \frac{2 \cdot N}{L \cdot t}$, where N is the number of intersections of the circle with dislocation lines, L – length of the circle, t – local thickness of the specimen at the area of the image. Following this analysis, the dislocation density amounts to 1.17E+12 m^{-2} and 2.57E+13 m^{-2} in SPS and AT&M tungsten, respectively.

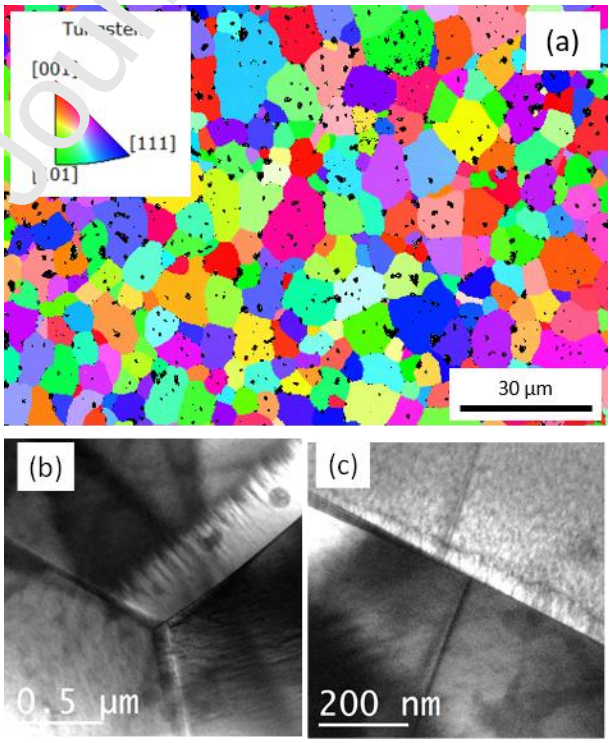


Fig. 2. (a) Normal direction (ND) Inverse pole figure (IPF) of SPS-produced tungsten. The equivalent grain diameter is 9.36 µm; (b) TEM micrograph showing triple junction grain boundary; (c) TEM micrograph showing high angle grain boundary and dislocation lines. Note the presence of black spots on the IPF map. These are pores, whose density is estimated to be 4E+14 m^{-3}, while the mean size is about 3-5 µm. This yields to about 4% porosity of the SPS material. The density determined by Archimedean method yield to 18.32 g/cm^3, corresponding to the porosity of 5%.

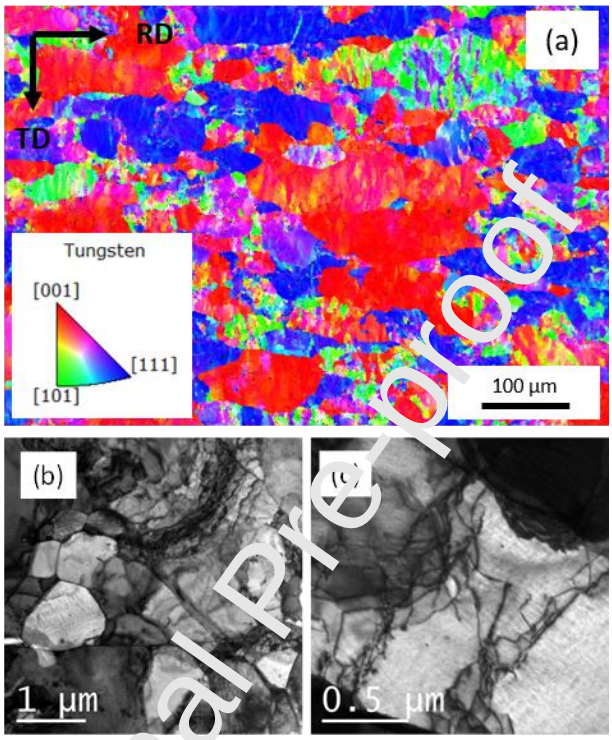


Fig. 3. (a) Normal direction (ND) Inverse pole figure (IPF) of AT&M tungsten. The equivalent grain diameter is 60.28 µm; (b) TEM micrograph showing several sub-grains; (c) TEM micrograph showing arrangement of dislocation lines inside a randomly selected sub-grain.

After mechanical tests the fracture surface was investigated by scanning electron microscopy (SEM; JEOL6610 – 15 kV, spot size of 50 with secondary electron detector). The qualitative and quantitative analyses of the microstructures of the fracture surfaces obtained after tensile, 3PB and FT tests were carried out by ImageJ image analysis software on SEM images at appropriate magnifications.

2.3 Mechanical testing procedures:

Two types of mechanical tests were performed here, namely: uniaxial tensile (TT) and fracture toughness test (FT). The tests were performed in air using the environmental furnace reaching maximum temperature of 600°C on a standard INSTRON 3800 universal mechanical test bench.

Journal Pre-proof

Uniaxial tensile tests were performed on small dog-bone shaped specimens, as shown in Fig.4. The overall length of the specimens is 16 mm with a gauge length of 5.2 mm and an effective cross section of 2.4 mm^2 (1.6 mm x 1.5 mm) or 2.88 mm^2 (1.6 mm x 1.8 mm). The strain was calculated based on the measurements of the pull rod displacement using linear variable differential transformer (LVDT). The LVDT and load cell were calibrated according to the required standards on the equipment applied to test both irradiated and reference samples. The gauge length to width ratio of 3.25 was in line with the ASTM standard value (being 4). Given the microstructure of the material (see Section 2.2), the thickness of the specimen cannot influence the mechanical response since sufficient number of grains is contained in the cross-section. The samples were cut by electric discharge machine using the wire of 20-50 µm and no special treatment was applied to the surface.

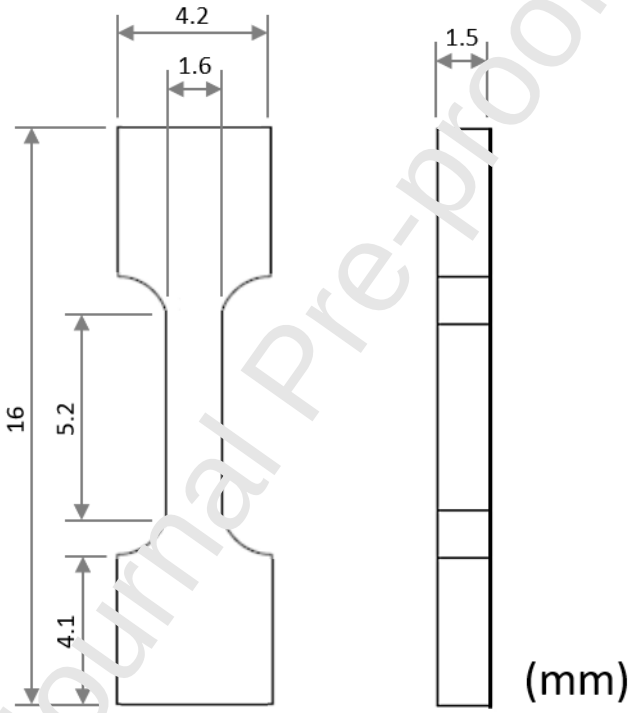


Fig. 4. Sketch of small dog-bone shaped specimens

Journal Pre-proof

Fracture Toughness

Disk-shaped compact tension (DCT) specimens with a narrow notch with a root radius around 50-90 µm were cut by EDM. The notch machined in the specimens for both materials is adapted to the T-L specimen fracture plane set-up, as imposed in the ASTM E399 standard [39]. The crack will propagate along the rolling direction on a plane normal to transversal direction. The sketch of the specimen and dimensions are shown in Fig.5 and Table 1.

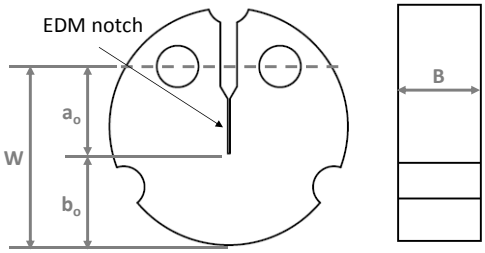


Fig. 5. Schematic showing the FT sample and characteristic dimension labels. The EDM notch is also shown. Three side grooves were applied to ensure proper centering of the sample in the irradiation capsule.

Table 1. Dimensions of DCT specimens.

	W	a_o	b_o	B
AT&M tungsten	~8.5 mm	~4.2 mm	~4.3 mm	~4 mm
SPS tungsten	~8.5 or ~8.8 mm	~4.2 mm	~4.3 or ~4.5 mm	~3 mm

The fracture toughness tests for irradiated and non-irradiated specimens were carried out in air using the same model of the test bench (INSTRON 3800) with the same type of an environmental furnace. The test temperature for irradiated specimens ranged from 400°C to 580°C. The reference measurements for the AT&M product are already reported in our previous work [22, 40].

K_Q values (linear elastic stress intensity factor) were calculated according to the requirements of the ASTM E399 [39]. Eq. (2) is used for the determination of the fracture toughness K_Q for mode I fracture which reads:

$$K_Q = \frac{P_Q}{B\sqrt{W}} \cdot f\left(\frac{a}{W}\right), \quad (2)$$

where P_Q is the fracture load if the specimens fracture without plastic deformation or the load intersected with the line with 0.95 slope of elastic region if plastic deformation happen, $f\left(\frac{a}{W}\right)$ is a geometry dependent function related to the ratio of a_o and W. The dimensional dependent function can be found form the standard.

2.4 Neutron irradiation

Neutron irradiation was performed in the Belgian Material Test Reactor (BR2). Fission reactors deliver mixed spectrum which imposes transmutation rates of W into Rhenium (Re) and Osmium (Os) to be essentially higher compared to those expected in ITER and DEMO conditions. As a result, the accelerated production of Re/Os yields to radiation induced precipitation as was discussed in refs. [41,

42] where the irradiation-induced microstructure after HFIR and JOYO irradiation was compared. To minimize the transmutation due thermal neutrons, the irradiation was performed inside the fuel element in the position close to the center of the reactor and in a mid-plane where the fast neutron (E > 0.1 MeV) flux is 7×10^{14}n/cm^2/s at a power of 60 MW. The samples were encapsulated in 1.5 mm steel tube filled with He. The thick stainless steel wall acts as additional shielding from the thermal neutrons. The gap between the samples and the tube was adjusted to achieve 600 ^{o}C following the thermal and neutronic calculations. The irradiation dose was 0.24 dpa, which was calculated by MCNPX 2.7.0 [43] based on the total fast neutron fluence. The dpa cross sections for W have been prepared from the JENDL4 file (MT444) for the threshold displacement energy of 55 eV, following the recommendation of IAEA [44]. The transmutation of Re and Os is calculated based on the ALEPH code developed by SCK•CEN and available nuclear databases [45-49] and for the irradiation position and spectrum the upper limit of the concentration (at%) of Re and Os is, respectively, 1.37% and 0.077%. Thus, the fraction of Os is about 5 % of the totally produced Re and Os.

Journal Pre-proof

3. Result

3.1 Tensile tests

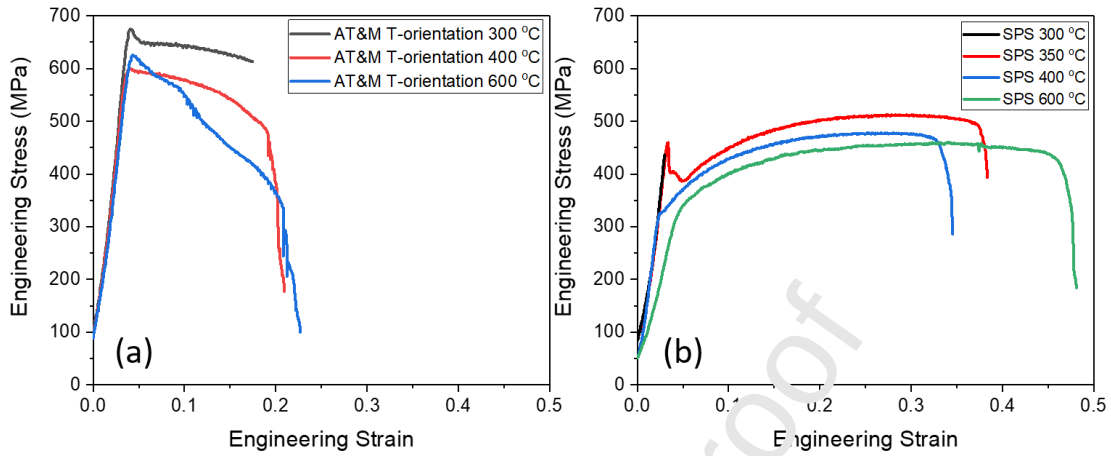


Fig.6. Comparison of stress-strain response of AT&M (a) and SPS (b) tungsten grades in the temperature range 300-600°C.

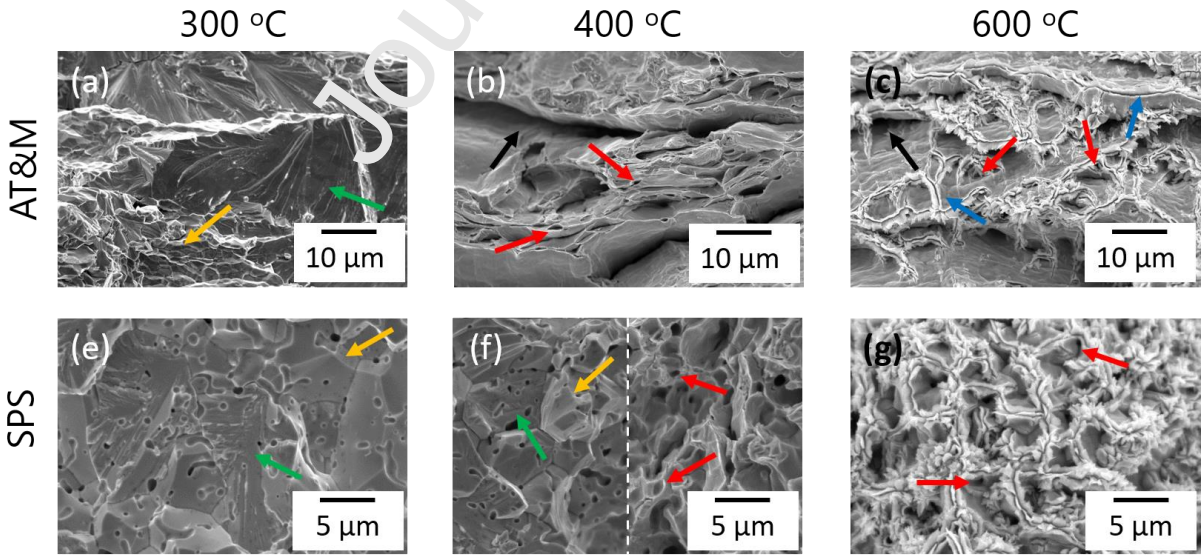
Table 2. Summary of tensile properties of SPS and AT&M tungsten grades.

Materials	Temp. (°C)	Yield strength (MPa)	Ultimate tensile strength (MPa)	Uniform elongation (%)	Total elongation (%)
SPS	350	437	513	24	35
	400	325	477	22	32
	600	321	458	27	43
AT&M	300	658	668	0	10
	400	590	599	1	19
	600	614	618	0	20

Fig. 6 shows the engineering stress-strain curves obtained for AT&M and SPS tungsten. Yield strength, ultimate tensile strength, uniform elongation, and total elongation are summarized in Table 2. Note that for AT&M tungsten, the data is produced for the T-orientation (corresponding to the situation when load is normal to the elongated grains, which is relevant for the assessment of the properties for ITER monoblock). Onset of ductile deformation is observed at 300 °C for AT&M and at 350 °C for SPS product. At 300°C, SPS product exhibits premature failure within elastic deformation limit. One can see that AT&M has rather low strain hardening capacity compared to the SPS product. This can be explained by initially high dislocation density and small sub-grain size in the microstructure of the

AT&M material, contrary to the SPS material. Furthermore, the SPS material shows very large uniform elongation and high strain hardening rate, which results in an increase of the flow stress by ~100 MPa moving from the yield strength to the ultimate tensile strength. In the case of AT&M material, the uniform elongation does not exceed 1% and the strain softening (decrease of engineering stress) is becoming more pronounced with increasing test temperature. Opposite to that, the capacity of the SPS material to absorb energy by plastic deformation rises with increasing the test temperature, proved by a larger uniform elongation and higher strain hardening measured at 600°C.

The reason why the swaged tungsten (i.e. AT&M) exhibits rather low uniform elongation could be explain by the orientation of the grains and reaction of the mechanical load, which is applied in the direction normal to the elongated grains. In this case, the plastic deformation yields to the formation of pile-ups nearby the high angle grain boundaries (HAGBs) yielding to the nucleation of micro-voids, whose coalescence results in the formation of micro-cracks [50]. The later propagate along high angle grain boundaries (because the plasticity is mostly penalized nearby the randomly mis-oriented HAGBs [51-53]), and given that the load is applied normal to the grain elongation, the micro-cracks coalesce into cracks resulting in the reduction of the effective cross-section of the sample. Correspondingly, the load required to continue the sample deformation starts to decrease. In the case of the SPS tungsten, the grain boundaries exhibit fine structure, which apparently facilitates the propagation of the plastic deformation across the sample delaying the formation of micro-cracks and thereby ensuring a large uniform elongation as soon as the temperature is sufficiently high for the movement and multiplication of the screw dislocations [54].



Yellow arrow: intergranular brittle fracture; Green arrow: transgranular brittle fracture;
Red arrow: dimples; Blue arrow: secondary cracks; **Black arrow**: delamination

Fig.7. Micrographs showing fracture surface of AT&M (a,b,c) and SPS (e,f,g) products as observed on the edges of broken tensile samples. The features related to deformation modes are specified by arrows with the legend underneath the SEM images.

The fracture surface of AT&M and SPS fractured tensile samples is shown in Fig. 7. Both materials show intergranular brittle fracture at 300 °C even though AT&M exhibits ductile deformation at this temperature. Besides intergranular brittle fracture, a large area of transgranular brittle fracture can be identified on the fracture surface of AT&M product. At 400 °C, dimples have been observed for both materials. However, delamination (intergranular grain debonding along the direction of load) has also been observed in AT&M due to the pancake shape of grains. Finally, secondary small cracks are found on the fracture surface for AT&M at 600 °C, while no such cracks were seen on the fully ductile SPS product.

3.2 Fracture toughness tests

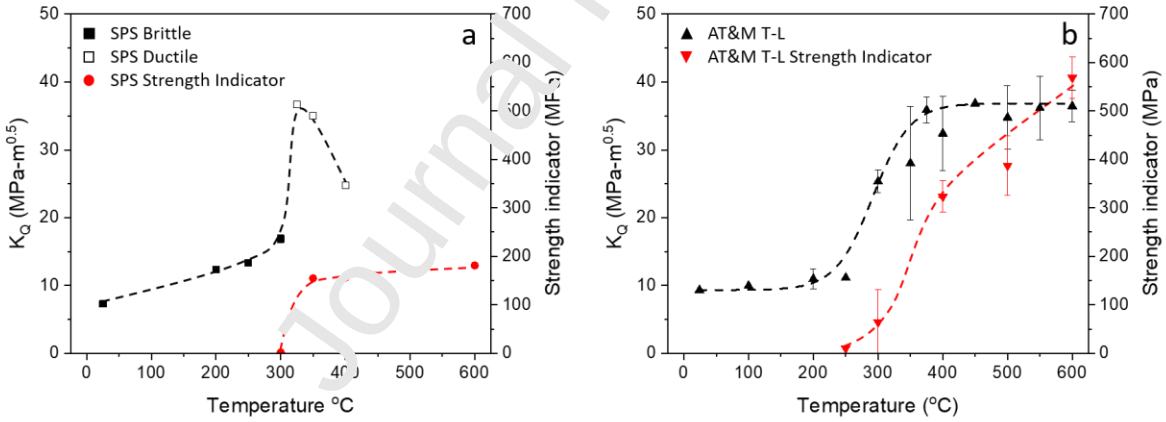


Fig.8. Fracture toughness (K_Q) and Strength Indicator calculated for SPS (a) and AT&M (b) products.

Fig.8 shows the fracture toughness and strength indicator for both materials as a function of temperature. The latter is the product of true fracture strength and true fracture strain, and it was used earlier by us to provide quantitative comparison of different tungsten grades showing different pattern of necking, for rationale see ref. [18]. The baseline fracture toughness in brittle state (i.e. room temperature) is about 7-10 MPa for both products. One can see a parabolic increase of the fracture toughness from the baseline up to ≥ 20 MPa·m$^{1/2}$ at 200°C and 300 °C for AT&M and SPS products, respectively. The saturation of the fracture toughness for AT&M is observed after reaching

400°C. For the SPS material, there is a reduction of K_Q above 325 °C, which is explained by the reduction of the yield strength. However, the fracture toughness in the ductile regime is not accounted for by K_Q and the contribution from the plastic deformation must also be included, which has much higher contribution compared to the energy coming in the elastic term. However, for the sake of comparison, we present K_Q for both materials.

Considering the strength indicator (i.e. product of the fracture strength and fracture strain), one can see that its function replicates the trend observed for the K_Q curves. In particular, there is a steep increase near the same temperature as where K_Q raises following the parabolic trend.

Following the results and discussion of earlier works done for commercially pure tungsten, the transition temperature (form brittle to ductile deformation) was defined as the temperature corresponding to the maximum of K_Q [55-57].The fracture toughness of SPS material increases from around 15 to 35 MPa·$m^{0.5}$ in a relatively narrow temperature region of 300-325°C. Such a sharp transition is consistent with the behavior of polycrystalline metals with body centered cubic lattice [50]. This transition is associated with the onset of plastic deformation governed by movement of screw dislocations and dislocation transmission through grain boundaries (to enable efficient dissipation of plastic deformation under external load) [21]. Given the relation between the absolute value of K_Q and the observed transition on the fracture surface of tensile samples, we shall use a criterion of $K_Q \geq 20$ MPa·$m^{0.5}$ as the onset transition region when discussing the results obtained for irradiated material. Due to the excessive cost of neutron irradiation and testing we did not perform tensile tests on the irradiated samples in the same conditions.

3.3 Fracture surface of SPS samples

Journal Pre-proof

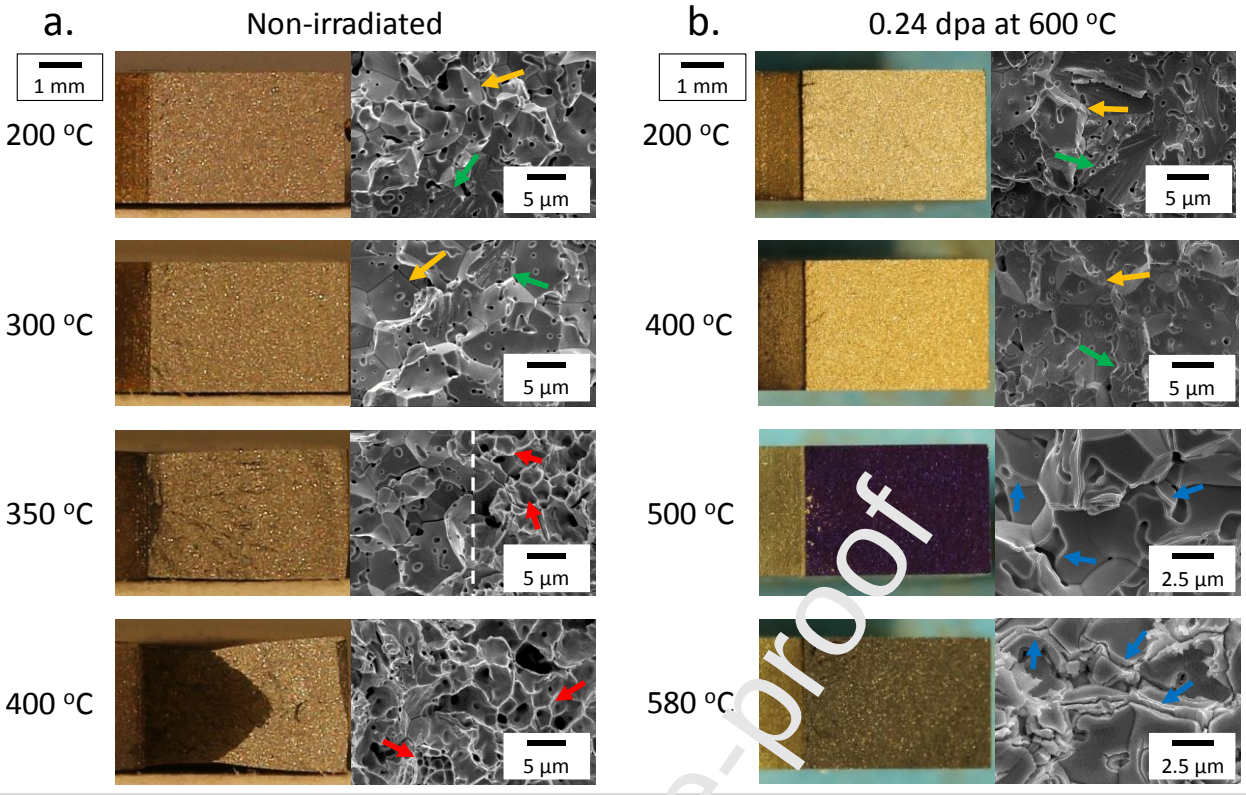


Fig.9. Micrographs showing fracture surfaces of SPS samples in non-irradiated (a, left column) and irradiated (b, right column) state. The features related to deformation modes are specified by arrows with the legend underneath the SEM images.

As shown in Fig. 9a, the fracture surface of non-irradiated SPS compact tension specimen evolves from the fully brittle flat pattern at 200 °C to the "V-shaped" profile, observed at 400°C. The latter pattern reflects the occurrence of the stable crack growth mode. Below 300 °C, the fracture surface contains a large portion of intergranular brittle fracture and small area of transgranular brittle fracture. Onset of stable tearing associated with dimples is observed at 350°C. However, the cleavage (with brittle fracture pattern) occurs right after a small distance of stable crack propagation. Thus, the transition from brittle crack advance to stable tearing resistance, for the employed DCT configuration, occurs within a temperature range of 300-400 °C.

3.4 Neutron irradiation effect

Journal Pre-proof

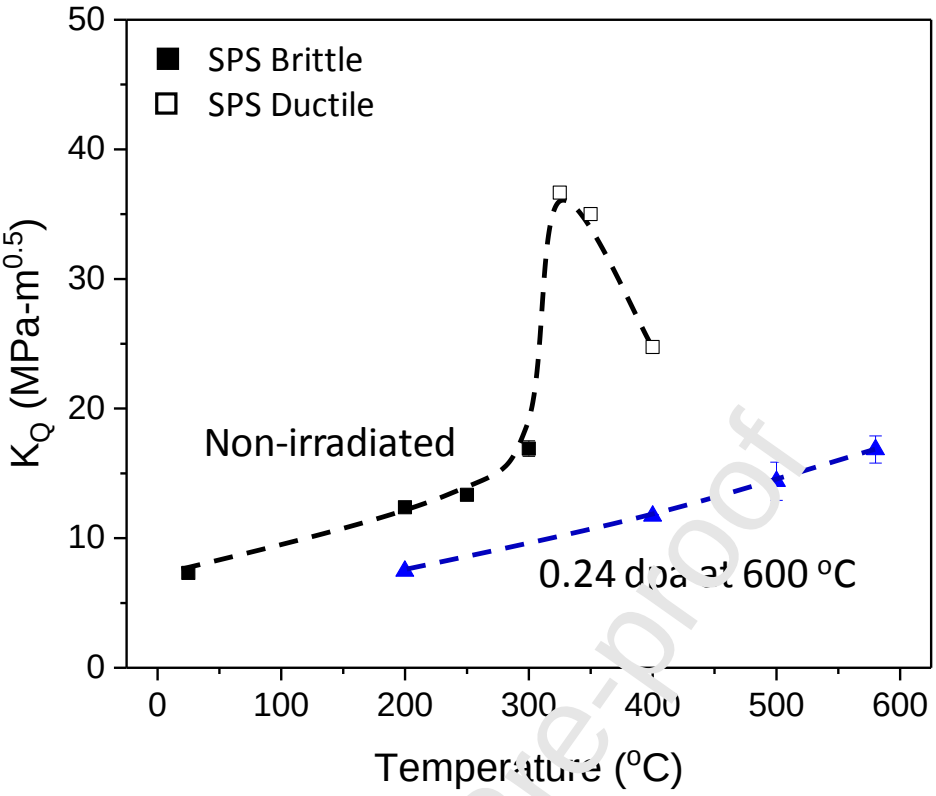


Fig.10. Fracture toughness (K_Q) for the SPS product before and after neutron irradiation.

Fig.10 present a comparison of the fracture toughness of reference and neutron irradiated SPS specimens. As one can see, after irradiation the fracture toughness continuously grows in the tested temperature range. The maximum K_Q, ~20 MPa-m$^{0.5}$, is achieved at 600°C (i.e. irradiation temperature). As was discussed before, it can be seen as an indication of the onset of the transition region. For all test temperatures, the fracture surface of the irradiated samples exhibits the intergranular brittle fracture pattern. However, as the test temperature exceed 500 °C, the secondary cracks on the grains bounding the crack tip can be observed, see Fig.9(b).

Now let us compare the fracture surface of reference and neutron irradiated specimens broken in the transition region (i.e. near K_Q~20 MPa-m$^{0.5}$). From Fig.9 (a) and (b), we see that the fracture surface of both samples (300°C for non-irradiated specimens and 580 °C for irradiated specimens) shows intergranular brittle fracture. However, as noted above the fracture surface of the irradiated sample contains small secondary cracks at the grain boundaries. We associate the presence of these small cracks and their branching with the development of local/confined plastic deformation nearby the crack tip. The plastic deformation region does not spread further than a single (or several) grain

boundary(ies) as apparently the slip transition is blocked by the presence of neutron irradiation defects in neighboring grains.

Secondary cracks are however not observed on the surface of the non-irradiated samples. We explain it by the fact that below the transition temperature, the crack extends without any significant plastic deformation. Whereas in the upper shelf (i.e. above 500°C), the stable tearing resistance, observed for the SPS material, excludes strong confinement of plastic deformation.

Finally, we discuss the absolute value of the fracture toughness and its reduction after the neutron irradiation. This discussion is provided by a comparison of K_{JC} for SPS and AT&M materials irradiated and tested in equivalent conditions. The only difference is the irradiation dose which samples were exposed to. The results are presented in Fig.11.

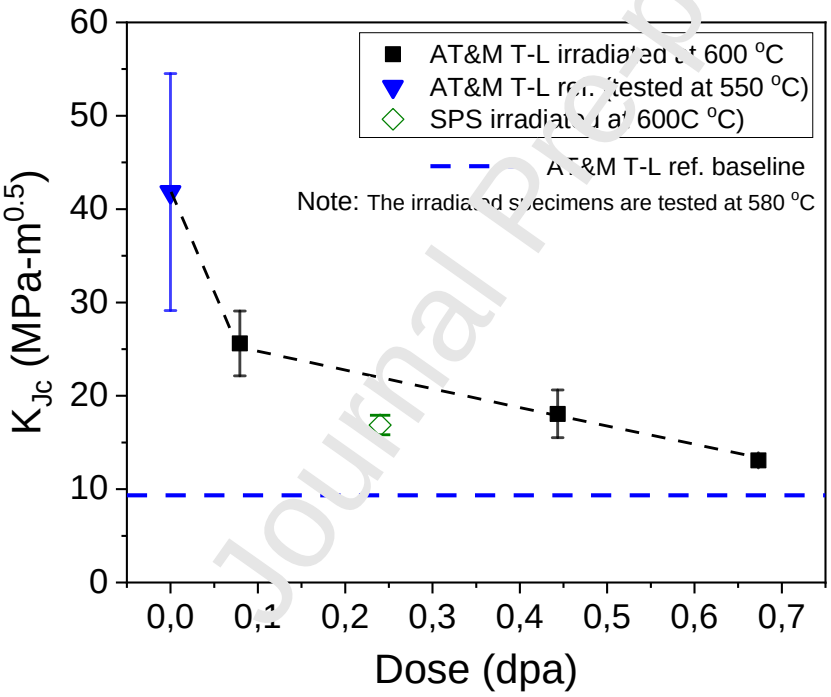


Fig.11. Fracture toughness of SPS and AT&M tungsten measured at test temperature of 580 °C as a function of the irradiation dose. Irradiation temperature is 600°C. The results for AT&M material are taken from [22, 37].

The fracture toughness, K_{Jc} i.e. elastic-plastic equivalent stress intensity factor, goes down with increasing the irradiation dose, as one can naturally expect. The trend of the reduction of K_{Jc} for AT&M is shown in the irradiation dose range up to ~0.7 dpa [37]. A dashed line is placed to guide an eye. By adding K_{Jc} measured for the SPS product we see that its value is located somewhat below the

trend line obtained for the AT&M material. Let us recall that the concentration of the Re accumulated in the AT&M material was about 0.6 at.% Re @ 0.08 dpa and 1.16 at.%Re @ 0.7 dpa. In the case of SPS material, the concentration of Re is calculated to be 1.37at.% at 0.24 dpa (due to the higher flux of thermal neutrons compared to the AT&M samples). At such transmutation rates and irradiation temperature, the irradiation damage is primary determined by the accumulation of the dislocation loops and nano-voids rather than by precipitation of Re and Os [42, 58]. The formation and growth of voids at 600 °C indeed take place [42], however, the peak swelling occurs around 800°C [35]. Thus, at 600°C at 0.24 dpa, we expect voids to have rather small size (due to the limited growth) and main contribution to the embrittlement should come from the dislocation loops. Investigation by transmission electron microscopy is planned for both types of materials and will be presented in upcoming works.

Journal Pre-proof

4. Summary and conclusive remarks

In this work, we have assessed tensile and fracture toughness properties of SPS-produced tungsten in the temperature region where brittleness of tungsten as ITER diverter PFC material plays important role. The results are discussed and compared with the data obtained for commercially pure W grade produced according to ITER specification (AT&M company) and tested in exactly the same conditions as the SPS product. The SPS product is also tested after neutron irradiation at 600°C at 0.24 dpa – close to the half end-of-life dose of the first wall divertor PFC. On the basis of the obtained results and discussion we can list the following statements:

- application of the SPS technology for the fabrication of bulk polycrystalline W delivers the product with the ductile to brittle transition temperature comparable to the commercially pure tungsten, even without post-processing thermo-mechanical optimization. In addition, SPS product offers essentially better tensile properties in terms of the uniform elongation as well as sufficiently high fracture toughness in the temperature range 350-600°C.

- neutron irradiation (at the fluence corresponding to 0.24 dpa) at 600°C causes the reduction of the fracture toughness in the whole studied temperature range (300-600°C) and apparent shift of the transition temperature by about 300°C, taking 20 MPa√m as an indicator of the onset of the transition region. Analysis of the fracture surface of the irradiated samples, tested at 600°C, confirms the presence of features corresponding to the ductile deformation.

- the reduction of the fracture toughness due to the neutron irradiation at 600°C was compared with recent data available for the AT&M commercially pure tungsten (irradiated and tested in equivalent conditions). The decrease of the fracture roughness observed in the SPS product is close to the trend curve deduced for the commercially pure tungsten.

Acknowledgement

This work has been carried out within the framework of the EUROfusion Consortium and has received funding from the Euratom research and training programme 2019–2020 under grant agreement No 633053. The views and opinions expressed herein do not necessarily reflect those of the European Commission. Part of the work was also supported by Czech Science Foundation through grant no. GA17-23154S.

Declaration of interests

The authors declare that they have no known competing financial interests or personal relationships that could have appeared to influence the work reported in this paper.

Journal Pre-proof

References:

[1] Stork D, Agostini P, Boutard JL, Buckthorpe D, Diegele E, Dudarev SL, et al. Developing structural, high-heat flux and plasma facing materials for a near-term DEMO fusion power plant: The EU assessment. J Nucl Mater. 2014;455:277-91.

[2] Hirai T, Panayotis S, Barabash V, Et.al. Use of tungsten material for the ITER divertor. Nuclear Materials and Energy. 2016;000:1-7.

[3] Federici G, Biel W, Gilbert MR, Kemp R, Taylor N, Wenninger R. European DEMO design strategy and consequences for materials. Nuclear Fusion. 2017;57.

[4] Pintsuk G. Tungsten as a Plasma-Facing material. 2012.

[5] Barabash V, Federici G, Rodig M, Snead LL, Wu CH. Neutron irradiation effects on plasma facing materials. Journal of Nuclear Materials. 2000;283:138-46.

[6] Coenen JW, Antusch S, Aumann M, Biel W, Du J, Engels J, et al. Materials for DEMO and reactor applications-boundary conditions and new concepts. Physica Scripta. 2016;T167.

[7] Rieth M, Armstrong D, Dafferner B, Heger S, Hoffmann A, Hofmann M-D, et al. Tungsten as a Structural Divertor Material. Advances in Science and Technology. 2010;73:11-21.

[8] Rieth M, al. e. A brief summary of the progress on the EFDA tungsten materials program. Journal of Nuclear Materials. 2013;442:S173-S80.

[9] Riesch J, Han Y, Almanstotter J, Coenen JW, Hoeschen T, Jasper B, et al. Development of tungsten fibre-reinforced tungsten composites towards their use in DEMO-potassium doped tungsten wire. Physica Scripta. 2016;T167.

[10] Zhang LH, Jiang Y, Fang QF, Xie ZM, Miao S, Zeng LF, et al. Microstructure and mechanical properties of tungsten composite reinforced by fibre network. Front Mater Sci. 2017;11:190-6.

[11] Xie ZM, Liu R, Miao S, Yang XD, Zhang T, Wang XP, et al. Extraordinary high ductility/strength of the interface designed bulk W-Zr-C alloy plate at relatively low temperature. Sci Rep-Uk. 2015;5.

[12] Blagoeva DT, Opschoor J, van der Laan JG, Sarbu C, Pintsuk G, Jong M, et al. Development of tungsten and tungsten alloys for DEMO divertor applications via MIM technology. Journal of Nuclear Materials. 2013;442:S198-S203.

[13] Matejicek J, Vilemova M, Nevrla B, Kocmanova L, Veverka J, Halasova M, et al. The influence of substrate temperature and spraying distance on the properties of plasma sprayed tungsten and steel coatings deposited in a shrouding chamber. Surf Coat Tech. 2017;318:217-23.

[14] Vassen R, Rauwald KH, Guillon O, Aktaa J, Weber T, Back HC, et al. Vacuum plasma spraying of functionally graded tungsten/EUROFER97 coatings for fusion applications. Fusion Engineering and Design. 2018;133:148-56.

[15] Gludovatz B, Wurster S, Hoffmann A, Pippan R. Fracture toughness of polycrystalline tungsten alloys. Int J Refract Met H. 2010;28:674-8.

[16] Wurster S, Gludovatz B, Pippan R. High temperature fracture experiments on tungsten-rhenium alloys. Int J Refract Met H. 2010;28:692-7.

Journal Pre-proof

[17] Gaganidze E, Rupp D, Aktaa J. Fracture behaviour of polycrystalline tungsten. Journal of Nuclear Materials. 2014;446:240-5.

[18] Yin C, Terentyev D, Pardoen T, Bakaeva A, Petrov R, Antusch S, et al. Tensile properties of baseline and advanced tungsten grades for fusion applications. Int J Refract Met H. 2018;75:153-62.

[19] Giannattasio A, Tanaka M, Joseph TD, Roberts SG. An empirical correlation between temperature and activation energy for brittle-to-ductile transitions in single-phase materials. Physica Scripta. 2007;T128:87-90.

[20] Lassila DH, Magness F, Freeman D. Ductile-Brittle Transition Temperature Testing of Tungsten Using the Three-Point Bend Test. Report Lawrence Livermore National Laboratory. 1991;UCRL-ID-108258.

[21] Giannattasio A, Yao Z, Tarleton E, Roberts SG. Brittle-ductile transitions in polycrystalline tungsten. Philosophical Magazine. 2010;90:3947-59.

[22] Yin C, Terentyev D, Pardoen T, Petrov R, Tong ZF. Ductile to brittle transition in ITER specification tungsten assessed by combined fracture toughness and bending tests analysis. Mat Sci Eng a-Struct. 2019;750:20-30.

[23] Nogami S, Watanabe S, Reiser J, Rieth M, Sickinger S, Hasegawa A. A review of impact properties of tungsten materials. Fusion Engineering and Design. 2018;135:196-203.

[24] Bonnekoh C, Hoffmann A, Reiser J. The brittle-to-ductile transition in cold rolled tungsten: On the decrease of the brittle-to-ductile transition by 600 K to-65 degrees C. Int J Refract Met H. 2018;71:181-9.

[25] Bonnekoh C, Jantsch U, Hoffmann J, Leiste H, Hartmaier A, Weygand D, et al. The brittle-to-ductile transition in cold rolled tungsten plates: Impact of crystallographic texture, grain size and dislocation density on the transition temperature. Int J Refract Met H. 2019;78:146-63.

[26] Zhang Y, Ganeev AV, Wang JT, Liu JQ, Alexandrov IV. Observations on the ductile-to-brittle transition in ultrafine-grained tungsten of commercial purity. Mat Sci Eng a-Struct. 2009;503:37-40.

[27] Miao S, Xie ZM, Yang XD, Liu R, Gao R, Zhang T, et al. Effect of hot rolling and annealing on the mechanical properties and thermal conductivity of W-0.5 wt.% TaC alloys. Int J Refract Met H. 2016;56:8-17.

[28] Faleschini M, Kreuzer H, Kiener D, Pippan R. Fracture toughness investigations of tungsten alloys and SPD tungsten alloys. Journal of Nuclear Materials. 2007;367:800-5.

[29] Farrell K, Schaffer AC, Stiegler JO. RECRYSTALLIZATION, GRAIN GROWTH AND THE DUCTILE-BRITTLE TRANSITION IN TUNGSTEN SHEET. J Less-Common Met. 1966;13:141-55.

[30] Nikolic V, Wurster S, Firneis D, Pippan R. Fracture toughness evaluation of UFG tungsten foil. Int J Refract Met H. 2018;76:214-25.

[31] Garrison LM, Katoh Y, Kumar NAPK. Mechanical properties of single-crystal tungsten irradiated in a mixed spectrum fission reactor. Journal of Nuclear Materials. 2019;518:208-25.

[32] Rieth M, Doerner R, Hasegawa A, Ueda Y, Wirtz M. Behavior of tungsten under irradiation and plasma interaction. Journal of Nuclear Materials. 2019;519:334-68.

Journal Pre-proof

[33] Steichen JM. Tensile Properties of Neutron-Irradiated Tzm and Tungsten. Journal of Nuclear Materials. 1976;60:13-9.

[34] Habainy J, Dai Y, Lee Y, Iyengar S. Mechanical properties of tungsten irradiated with high-energy protons and spallation neutrons. Journal of Nuclear Materials. 2019;514:189-95.

[35] Matolich J, Nahm H, Moteff J. Swelling in neutron irradiated tungsten and tungsten-25 rhenium. Scripta Metall Mater. 1974;8:837-42.

[36] Castin N, Bakaev A, Bonny G, Sand AE, Malerba L, Terentyev D. On the onset of void swelling in pure tungsten under neutron irradiation: An object kinetic Monte Carlo approach. Journal of Nuclear Materials. 2017;493:280-93.

[37] Yin C, Terentyev D, Van Dyck S, Stankovskiy A, Petrov RH, Pardoen T. Effect of high temperature neutron irradiation on fracture toughness of ITER-specification tungsten. Physica Scripta. 2019;Submitted.

[38] Butler TW. Report E-69-1 on the determination of dislocation densities. Annapolis, Maryland: United States Naval Academy Engineering Department; 1969.

[39] ASTM. Standard test method for linear-elastic plane strain fracture toughness KIC of metallic materials. E 399-12: ASTM international; 2012.

[40] Yin C, Terentyev D, Pardoen T, Petrov R, Tong Z. Ductile to brittle transition in ITER specification tungsten assessed by combined fracture toughness and bending tests analysis. Materials Science & Engineering: A. 2019;750:20-30.

[41] Koyanagi T, Kumar NAPK, Hwang T, Garrison LM, Hu XX, Snead LL, et al. Microstructural evolution of pure tungsten neutron irradiated with a mixed energy spectrum. Journal of Nuclear Materials. 2017;490:66-74.

[42] Hasegawa A, Fukuda M, Yabuuchi K, Nogami S. Neutron irradiation effects on the microstructural development of tungsten and tungsten alloys. Journal of Nuclear Materials. 2016;471:175-83.

[43] Pelowitz D, Durkee J, Elson J, Fensin M, James M, Johns R, et al. MCNPX 2.7. 0 Extensions. LA-UR-11-02295 ed: Los Alamos National Laboratory; 2011.

[44] Dudarev SL, "DPA definition and estimates," https://www-amdis.iaea.org/CRP/IrradiatedTungsten/RCM2/RCM2Presentation-DudarevDPA-2015-09-10.pdf).

[45] Stankovskiy A, Van den Eynde G, Fiorito L. ALEPH V.2.7, A Monte Carlo Burn-Up Code. ALEPH V.2.7 ed: SCK•CEN; 2018.

[46] Plompen A, et al. The joint evaluated fission and fusion nuclear data library, JEFF-3.3. In: Journal EP, editor.To be published.

[47] Brown DA, Chadwick M, Capote R, Kahler A, Trkov A, Herman M, et al. ENDF/B-VIII. 0: the 8th major release of the nuclear reaction data library with CIELO-project cross sections, new standards and thermal scattering data. Nuclear Data Sheets. 2018;148:1-142.

[48] Konobeyev AY, Fischer U, Korovin YA, Simakov S. Evaluation of effective threshold displacement energies and other data required for the calculation of advanced atomic displacement cross-sections. Nuclear Energy and Technology. 2017;3:169-75.

Journal Pre-proof

[49] Norgett M, Robinson M, Torrens I. A proposed method of calculating displacement dose rates. Nuclear engineering and design. 1975;33:50-4.

[50] Hull D, Bacon DJ. Introduction to dislocations. Oxford: Butterworth-Heinemann; 2001.

[51] Terentyev D, Bakaev A, Serra A, Pavia F, Baker KL, Anento N. Grain boundary mediated plasticity: The role of grain boundary atomic structure and thermal activation. Scripta Materialia. 2018;145:1-4.

[52] Sheng H, Van Oost G, Zhurkin E, Terentyev D, Dubinko VI, Uytdenhouwen I, et al. High temperature strain hardening behavior in double forged and potassium doped tungsten. Journal of Nuclear Materials. 2014;444:214-9.

[53] Dubinko A, Terentyev D, Bakaeva A, Verbeken K, Wirtz M, Hernandez-Mayoral M. Evolution of plastic deformation in heavily deformed and recrystallized tungsten of ITER specification studied by TEM. Int Journal of Refractory Metals and Hard Materials. 2017;66:105-15.

[54] Terentyev D, Xiao XZ, Dubinko A, Bakaeva A, Duan HL. Dislocation-mediated strain hardening in tungsten: Thermo-mechanical plasticity theory and experimental validation. Journal of the Mechanics and Physics of Solids. 2015;85:1-15.

[55] Gumbsch P. Brittle fracture and the brittle-to-ductile transition of tungsten. J Nucl Mater. 2003;323:304-12.

[56] Gumbsch P, Riedle J, Hartmaier A, Fischmeister HF. Controlling factors for the brittle-to-ductile transition in tungsten single crystals. Science. 1998;282:1293-5.

[57] Rupp D, Weygand SM. Loading rate dependence of the fracture toughness of polycrystalline tungsten. J Nucl Mater. 2011;417:477-80.

[58] Fukuda M, Kumar NAPK, Koyanagi T, Garrison LM, Snead LL, Katoh Y, et al. Neutron energy spectrum influence on irradiation hardening and microstructural development of tungsten. Journal of Nuclear Materials. 2016;479:249-54.

Journal Pre-proof

Journal Pre-proof

Highlights

- Fracture toughness of SPS tungsten before and after irradiation is assessed
- neutron irradiation at end-of-life PFC component increases DBTT by 300^{o}C
- SPS tungsten exhibit similar performance as powder metallurgy tungsten

Journal Pre-proof